Supporting Information

Aggregation-Induced Delayed Fluorescence Luminogens with Accelerated Reverse Intersystem Crossing for High-Performance OLEDs

Jingwen Xu,[1,‡] Xiangyu Zhu,[1,‡] Jingjing Guo,[1] Jianzhong Fan,[2] Jiajie Zeng,[1] Shuming Chen,[3] Zujin Zhao,*[,1] and Ben Zhong Tang[1,4]

[1] State Key Laboratory of Luminescent Materials and Devices, Key Laboratory of Luminescence from Molecular Aggregates of Guangdong Province, South China University of Technology, Guangzhou 510640, China. E-mail: mszjzhao@scut.edu.cn

[2] Shandong Province Key Laboratory of Medical Physics and Image Processing Technology, Institute of Materials and Clean Energy, School of Physics and Electronics, Shandong Normal University, Jinan 250014, China

[3] Department of Electrical and Electronic Engineering, South University of Science and Technology of China, Shenzhen, Guangdong 518055, China

[4] Department of Chemistry, The Hong Kong University of Science & Technology, Clear Water Bay, Kowloon, Hong Kong, China

Contents

General Information

All the chemicals and reagents were purchased from commercial sources and used as received without further purification. The final products were subjected to vacuum sublimation to further improve purity before photoluminescence (PL) and electroluminescence (EL) properties investigations. ^{1}H and ^{13}C NMR spectra were measured on a Bruker AV 400 or 500 spectrometer in $CDCl_3$ at room temperature. High resolution mass spectra (HRMS) were recorded on a GCT premier CAB048 mass spectrometer operating in MALDI-TOF mode. Single crystal X-ray diffraction intensity data were collected on a Bruker–Nonices Smart Apex CCD diffractometer with graphite monochromated MoKα radiation. Processing of the intensity data was carried out using the SAINT and SADABS routines, and the structure and refinement were conducted using the SHELTL suite of X-ray programs (version 6.10). UV-vis absorption spectra were measured on a Shimadzu UV-2600 spectrophotometer. PL spectra were recorded on a Horiba Fluoromax-4 spectrofluorometer. Fluorescence quantum yields were measured using a Hamamatsu absolute PL quantum yield spectrometer C11347 Quantaurus_QY. The room temperature transient PL decay spectra were measured using Quantaurus-Tau fluorescence lifetime measurement system (C11367-03, Hamamatsu Photonics Co., Japan). The temperature-dependent transient PL decay spectra were measured using FLS980 fluorometer (Edinburgh Instruments). Cyclic voltammetry (CV) was measured in a solution of tetra-*n*-butylammonium hexafluorophosphate (Bu_4NPF_6, 0.1 M) in dichloromethane or *N*,*N*-dimethylformamide containing the sample at a scan rate of 100 mV s^{-1}. Three-electrode system (Ag/Ag^+, platinum wire and glassy carbon electrode as reference, counter and work electrode respectively) was used in the CV method (HOMO = –[E_{ox} + 4.8] eV; LUMO = –[E_{re} + 4.8] eV). E_{ox} and E_{re} represent the onset oxidation and reduction potentials relative to F_c/F_c^+, respectively. Platinum electrode coated with thin molecule film was used as the working electrode. The ground-state geometries were optimized by density functional theory (DFT) method and the photophysical properties of excited states were studied by time-dependent density functional theory (TDDFT) at the M06-2X/6-31G* level.[1] The combined quantum mechanics and molecular mechanics (QM/MM)[2] method with two-layer ONIOM approach was used to simulate the properties in solid state, treating crystal structures as the initial configurations. All of these calculations were carried out in the Gaussian 09 package. Based on the optimized geometries, the SOC values between

S_1 and T_1 in gas and solid phase were calculated employing the basis set 6-31G* by the Dalton 2013 package.

Syntheses and Characterization

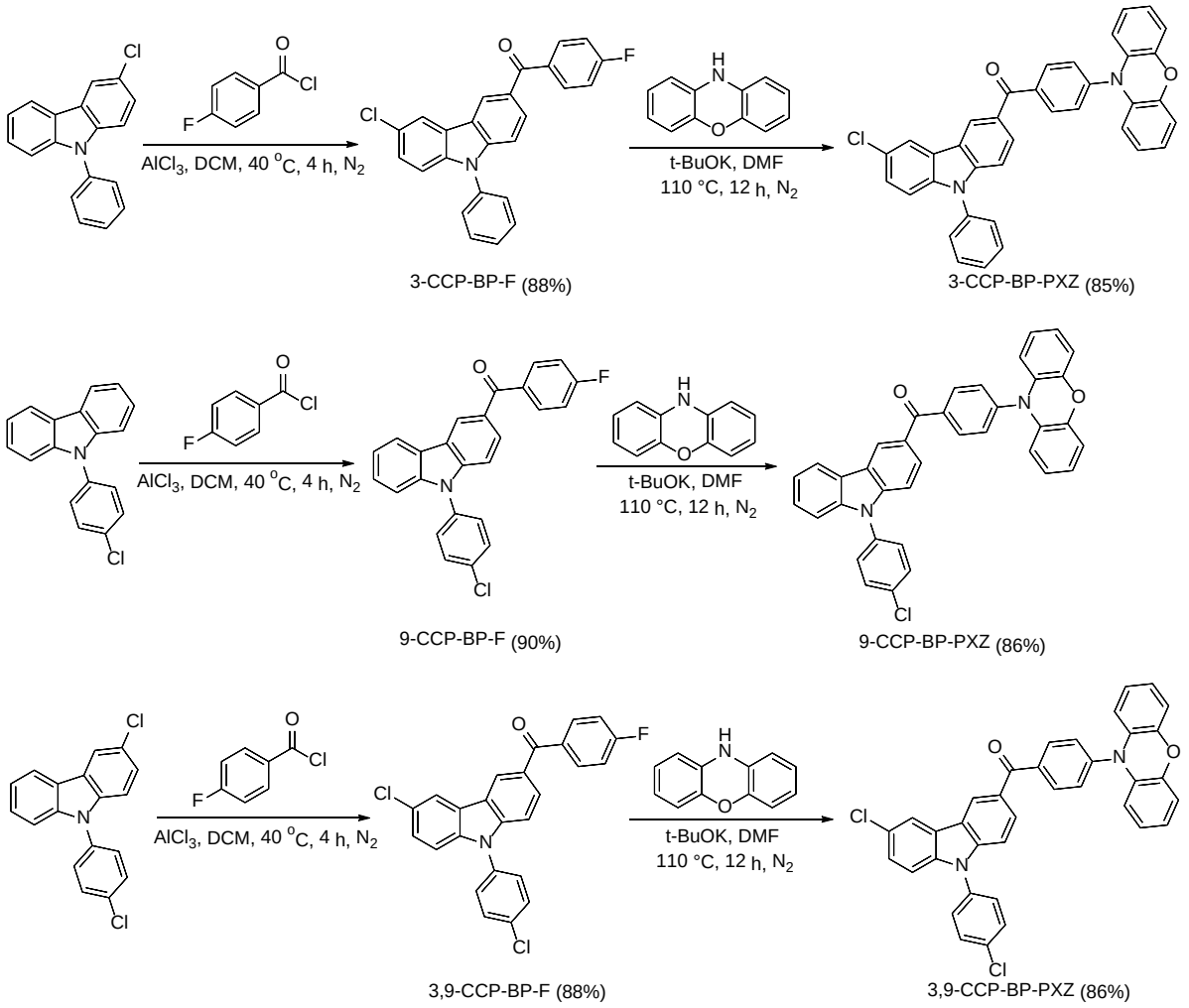

Scheme S1. Synthetic routes of 3-CCP-BP-PXZ, 9-CCP-BP-PXZ and 3,9-CCP-BP-PXZ.

(6-Chloro-9-phenyl-9H-carbazol-3-yl)(4-fluorophenyl)methanone (3-CCP-BP-F): 3-Chloro-9-phenyl-9H-carbazole (0.83 g, 3.0 mmol), 4-fluorobenzoyl chloride (0.57 g, 3.6 mmol) and $AlCl_3$ (0.48 g, 3.6 mmol) were mixed together under stirring in dehydrated dichloromethane (20 mL) in ice bath for 15 min. The mixture was reacted at 40 °C for 4 h. Then, the reaction was quenched with ice water and hydrochloric acid (30 mL, 2:1 v/v), and extracted with dichloromethane. The combined organic layers were combined and washed with water three times, and dried over

anhydrous $MgSO_4$. After filtration and solvent evaporation under reduced pressure, the residue was purified by silica-gel column chromatography using dichloromethane/petroleum as eluent. 3-CCP-BP-F was obtained as a white solid in 88% yield. ^{1}H NMR (400 MHz, $CDCl_3$) δ 8.55 (d, *J* = 1.2 Hz, 1H), 8.11 (d, *J* = 2.0 Hz, 1H), 7.97–7.92 (m, 1H), 7.92–7.85 (m, 2H), 7.69–7.61 (m, 2H), 7.58–7.50 (m, 3H), 7.46–7.37 (m, 2H), 7.32 (d, *J* = 8.0 Hz, 1H), 7.24–7.16 (m, 2H). ^{13}C NMR (100 MHz, $CDCl_3$) δ 194.96, 166.39, 163.87, 143.80, 140.11, 136.53, 134.80, 132.53, 132.44, 130.25, 129.77, 128.99, 128.48, 127.07, 126.92, 126.51, 124.51, 123.95, 122.03, 120.39, 115.56, 115.34, 111.38, 109.86. HRMS: *m/z* [M^+] calcd for $C_{25}H_{15}ClFNO$, 399.0826; found, 399.0839.

(4-(10H-Phenoxazin-10-yl)phenyl)(6-chloro-9-phenyl-9H-carbazol-3-yl)methanone (3-CCP-BP-PXZ): A mixture of 3-CCP-BP-F (0.40 g, 1.0 mmol), phenoxazine (0.27 g, 1.5 mmol) and potassium *tert*-butoxide (0.22 g, 2 mmol) were stirred for 15 min in deaerated and dehydrated *N*,*N*-dimethylformamide (20 mL) under nitrogen at room temperature. Then the reaction mixture was heated up to 110 °C and reacted for 12 h. After cooled to room temperature, the reaction mixture was poured into a large amount of water and extracted with dichloromethane. The combined organic layers were washed with water for three times and dried over anhydrous $MgSO_4$. After filtration and solvent evaporation, the residue was purified by silica-gel column chromatography using dichloromethane/petroleum ether as an eluent. 3-CCP-BP-PXZ was obtained as a yellow solid in 85% yield. ^{1}H NMR (500 MHz, $CDCl_3$) δ 8.73 (d, *J* = 1.4 Hz, 1H), 8.21 (d, *J* = 7.7 Hz, 1H), 8.08 (d, *J* = 8.3 Hz, 2H), 7.99 (m, 1H), 7.82–7.74 (m, 2H), 7.57–7.45 (m, 5H), 7.45–7.35 (m, 3H), 6.84–6.51 (m, 6H), 6.05 (m, 2H). ^{13}C NMR (100 MHz, $CDCl_3$) δ 195.37, 144.00, 143.28, 142.45, 141.51, 139.36, 138.62, 135.92, 133.84, 133.39, 132.68, 130.76, 129.39, 128.83, 128.78, 127.07, 123.77, 123.43, 123.34, 123.30, 121.83, 121.77, 121.30, 120.85, 115.67, 113.38, 110.11, 109.32. HRMS: *m/z* [M^+] calcd for $C_{37}H_{23}ClN_2O_2$, 562.1448; found, 562.1459.

(9-(4-Chlorophenyl)-9H-carbazol-3-yl)(4-fluorophenyl)methanone (9-CCP-BP-F): Following the procedure described for 3-CCP-BP-F, the compound 9-CCP-BP-F was made from 9-(4-chlorophenyl)-9H-carbazole (0.83 g, 3.0 mmol), 4-fluorobenzoyl chloride (0.57 g, 3.6 mmol) and $AlCl_3$ (0.48 g, 3.6 mmol) as a white solid. Yield: 90%. ^{1}H NMR (500 MHz, $CDCl_3$) δ 8.62 (d, *J* = 1.3 Hz, 1H), 8.16 (d, *J* = 7.5 Hz, 1H), 7.94–7.85 (m, 3H), 7.66–7.59 (m, 2H), 7.55–7.50 (m, 2H), 7.47 (m, 1H), 7.42–7.33 (m, 3H), 7.24–7.16 (m, 2H). ^{13}C NMR (100 MHz, $CDCl_3$) δ 195.11, 166.36, 163.84, 143.23, 141.59, 135.46, 134.94, 134.91, 133.92, 132.54, 132.46, 130.41, 129.72, 128.63,

128.47, 126.99, 123.72, 123.43, 123.19, 121.22, 120.78, 115.50, 115.29, 110.09, 109.28. HRMS: *m/z* [M^+] calcd for $C_{25}H_{15}ClFNO$, 399.0826; found, 399.0839.

(4-(10H-Phenoxazin-10-yl)phenyl)(9-(4-chlorophenyl)-9H-carbazol-3-yl)methanone (9-CCP-BP-PXZ): Following the procedure described for 3-CCP-BP-PXZ, the compound 9-CCP-BP-PXZ was made from 9-CCP-BP-F (0.40 g, 1.0 mmol), phenoxazine (0.27 g, 1.5 mmol) and potassium *tert*-butoxide (0.22 g, 2 mmol) as a yellow solid. Yield: 86%. ^{1}H NMR (500 MHz, $CDCl_3$) δ 8.73 (d, *J* = 1.4 Hz, 1H), 8.21 (d, *J* = 7.7 Hz, 1H), 8.10–8.06 (m, 2H), 8.00 (m, 1H), 7.67–7.59 (m, 2H), 7.56–7.50 (m, 4H), 7.47 (m, 1H), 7.43 (d, *J* = 8.6 Hz, 1H), 7.41–7.35 (m, 2H), 6.77–6.61 (m, 6H), 6.05 (m, 2H). ^{13}C NMR (125 MHz, $CDCl_3$) δ 195.37, 144.02, 143.39, 142.47, 141.62, 138.65, 135.41, 133.96, 133.87, 132.68, 130.75, 130.41, 129.39, 128.83, 128.46, 127.06, 123.77, 123.42, 123.31, 121.78, 121.28, 120.85, 115.69, 113.39, 110.12, 109.32. HRMS: *m/z* [M^+] calcd for $C_{37}H_{23}ClN_2O_2$, 562.1448; found, 562.1462.

(6-Chloro-9-(4-chlorophenyl)-9H-carbazol-3-yl)(4-fluorophenyl)methanone (3,9-CCP-BP-F): Following the procedure described for 3-CCP-BP-F, the compound 3,9-CCP-BP-F was made from 3-chloro-9-(4-chlorophenyl)-9H-carbazole (0.93 g, 3.0 mmol), 4-fluorobenzoyl chloride (0.57 g, 3.6 mmol) and $AlCl_3$ (0.48 g, 3.6 mmol) as a white solid. Yield: 88%. ^{1}H NMR (500 MHz, $CDCl_3$) δ 8.54 (d, *J* = 1.4 Hz, 1H), 8.10 (d, *J* = 2.0 Hz, 1H), 7.96–7.93 (m, 1H), 7.90–7.85 (m, 2H), 7.67–7.59 (m, 2H), 7.51–7.47 (m, 2H), 7.42–7.37 (m, 2H), 7.30–7.18 (m, 3H). ^{13}C NMR (100 MHz, $CDCl_3$) δ 195.15, 144.01, 143.73, 142.66, 139.93, 138.35, 135.01, 134.28, 133.81, 132.68, 130.81, 130.53, 129.72, 129.29, 128.36, 127.14, 126.83, 124.58, 123.97, 123.32, 122.27, 121.81, 120.57, 115.70, 113.41, 111.17, 109.70. HRMS: *m/z* [M^+] calcd for $C_{25}H_{14}Cl_2FNO$, 433.0436; found, 433.0446.

(4-(10H-Phenoxazin-10-yl)phenyl)(6-chloiro-9-(4-chlorophenyl)-9H-carbazol-3-yl)methanone (3,9-CCP-BP-PXZ): Following the procedure described for 3-CCP-BP-PXZ, the compound 3,9-CCP-BP-PXZ was made from 3,9-CCP-BP-F (0.43 g, 1.0 mmol), phenoxazine (0.27 g, 1.5 mmol) and potassium *tert*-butoxide (0.22 g, 2 mmol) as a yellow solid. Yield: 86%. ^{1}H NMR (500 MHz, $CDCl_3$) δ 8.66 (d, *J* = 4.0 Hz, 1H), 8.15 (d, *J* = 2.0 Hz, 1H), 8.09–8.06 (m, 2H), 8.03 (m, 1H), 7.64–7.61 (m, 2H), 7.55–7.49 (m, 4H), 7.44–7.28 (m, 3H), 6.74–6.63 (m, 6H), 6.05 (m, 2H). ^{13}C NMR (125 MHz, $CDCl_3$) δ 195.12, 144.02, 143.74, 142.66, 139.95, 138.38, 135.02, 134.29, 132.68, 130.54, 130.41, 129.75, 129.29, 128.45, 128.37, 127.15, 126.85, 124.59, 123.97, 123.32, 122.28, 121.82, 120.58, 115.70, 113.41, 111.18, 109.70. HRMS: *m/z* [M^+] calcd for $C_{37}H_{22}Cl_2N_2O_2$,

596.1058; found, 596.1071.

X-Ray Crystallography

Crystal data for 3-CCP-BP-PXZ (CCDC 1923315): $C_{37}H_{23}ClN_2O_2$, M_W = 563.02, monoclinic, P21/c, a = 18.4693(9), b = 14.2675(9), c = 10.2068(6) Å, α = 90°, β = 93.438(5)°, γ = 90°, V = 2684.8(3) Å^3, Z = 4, Dc = 1.393 g cm^{-3}, μ = 0.182 mm^{-1} (MoKα, λ = 0.71073), F(000) = 1168, T = 173(2) K, $2\theta_{max}$ = 26.998^o (98.9%), 25732 measured reflections, 5798 independent reflections (R_{int} = 0.0628), GOF on F^2 = 1.043, R_1 = 0.0882, wR_2 = 0.1162 (all data), Δe 0.287 and –0.299 eÅ^{-3}.

Crystal data for 9-CCP-BP-PXZ (CCDC 1923317): $C_{37}H_{23}ClN_2O_2 \cdot CH_3OH$, M_W = 595.06, triclinic, P-1, a = 9.4665(4), b = 9.7493(4), c = 17.7296(6) Å, α = 76.693(3)°, β = 85.112(3)°, γ = 65.190(4)°, V = 1445.27(11) Å^3, Z = 2, Dc = 1.367 g cm^{-3}, μ = 0.176 mm^{-1} (MoKα, λ = 0.71073), F(000) = 620, T = 173(2) K, $2\theta_{max}$ = 26.998^o (98.4%), 22776 measured reflections, 6211 independent reflections (R_{int} = 0.0426), GOF on F^2 = 1.040, R_1 = 0.0724, wR_2 = 0.1319 (all data), Δe 0.468 and –0.471 eÅ^{-3}.

Crystal data for 3,9-CCP-BP-PXZ (CCDC 1923323): $C_{37}H_{22}Cl_2N_2O_2 \cdot CH_2Cl_2$, M_W = 682.39, monoclinic, P21/n, a = 8.673(2), b = 9.912(2), c = 36.418(9) Å, α = 90°, β = 90.161(4)°, γ = 90°, V = 3130.8(13) Å^3, Z = 4, Dc = 1.448 g cm^{-3}, μ = 0.418 mm^{-1} (MoKα, λ = 0.71073), F(000) = 1400, T = 158(2) K, $2\theta_{max}$ = 25.562^o (98.0%), 21843 measured reflections, 5738 independent reflections (R_{int} = 0.0910), GOF on F^2 = 1.073, R_1 = 0.1567, wR_2 = 0.2121 (all data), Δe 0.417 and –0.868 eÅ^{-3}.

OLED Fabrication and Characterization

Glass substrates pre-coated with a 90-nm-thin layer of indium tin oxide (ITO) with a sheet resistance of 15–20 Ω per square were completely cleaned in ultrasonic bath of detergent and deionized water, respectively, each step takes 30 minutes. After that, the substrates were dried in a 65 ^{o}C oven. Then, the substrates were treated by O_2 plasma for 10 minutes to improve the hole injection capacity of ITO. The vacuum-deposited OLEDs were constructed under a pressure of < 5 × 10^{-4} Pa. Organic materials, LiF and Al were deposited with the rates of 1–2 Å s^{-1}, 0.1 Å s^{-1} and 10 Å s^{-1}, respectively. The effective emitting area of the device was 4 mm^2. All the device characterizations were carried out at room temperature under ambient laboratory conditions without any additional encapsulation,

as soon as the devices were fabricated. EL spectra were obtained in normal direction via a spectrometer (Ocean Optics USB 2000+), according to the method reported by S. R. Forrest.[3] Current density-voltage-luminance and external quantum efficiency were characterized with a dual-channel Keithley 2614B source meter and a PIN-25D silicon photodiode.

Additional Data

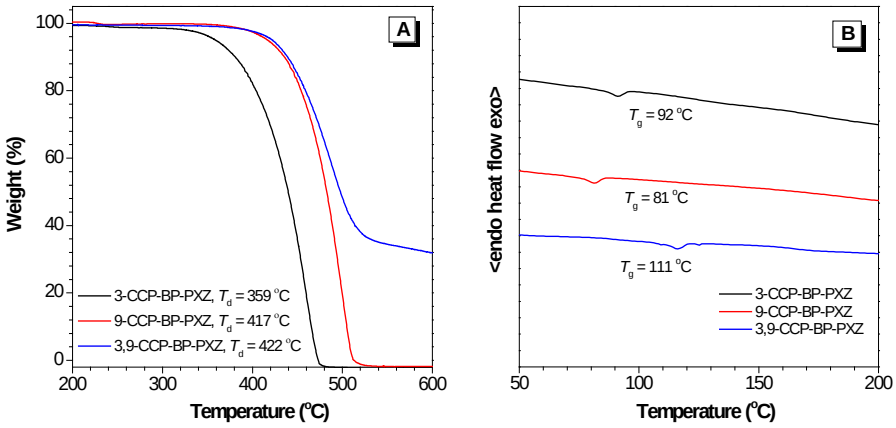

Figure S1. (A) TGA and (B) DSC thermograms of 3-CCP-BP-PXZ, 9-CCP-BP-PXZ and 3,9-CCP-BP-PXZ, recorded under nitrogen at a heating rate of (A) 20 and (B) 10 °C min^{-1}, respectively. T_g is the glass-transition temperature; T_d is the decomposition temperature.

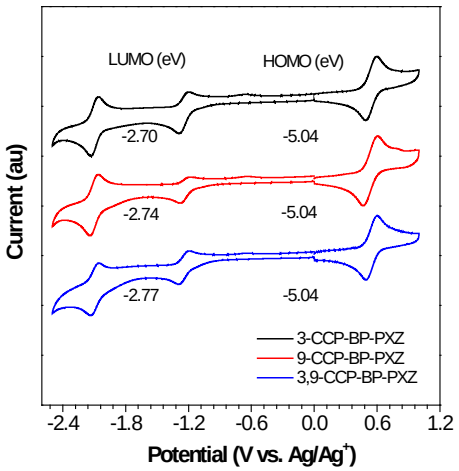

Figure S2. Cyclic voltammograms of 3-CCP-BP-PXZ, 9-CCP-BP-PXZ and 3,9-CCP-BP-PXZ measured in dichloromethane or *N*,*N*-dimethylformamide containing 0.1 M tetra-*n*-butylammonium hexafluorophosphate. Scan rate: 100 mV s^{-1}.

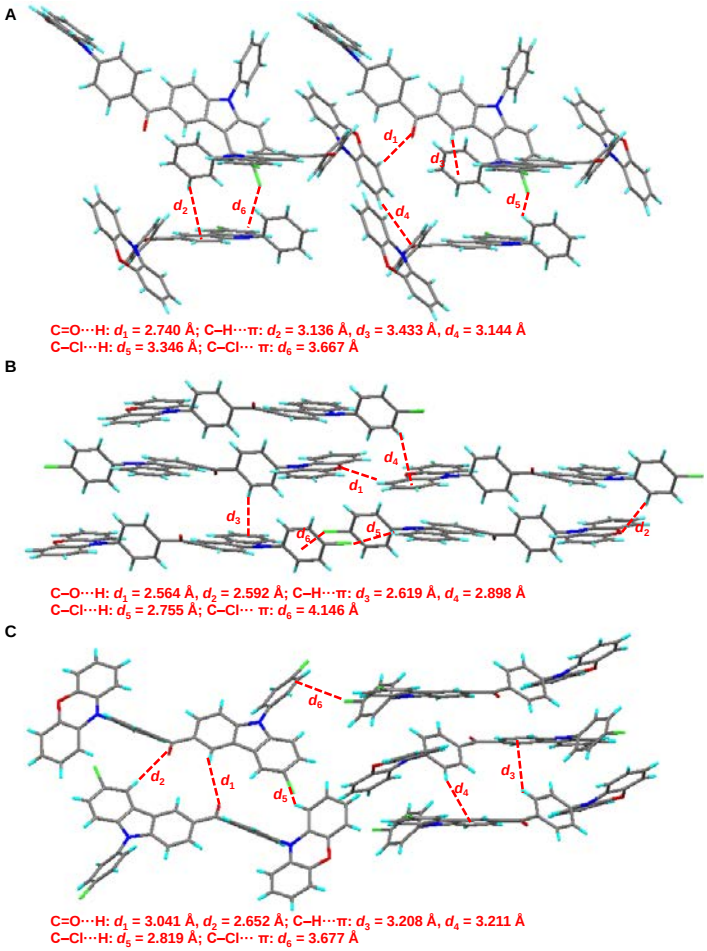

Figure S3. Molecular packing of 3-CCP-BP-PXZ, 9-CCP-BP-PXZ and 3,9-CCP-BP-PXZ in crystals with indicated distances (Å) of C–H···π, C–Cl···π, C–Cl···H, C–O···H and C=O···H interactions.

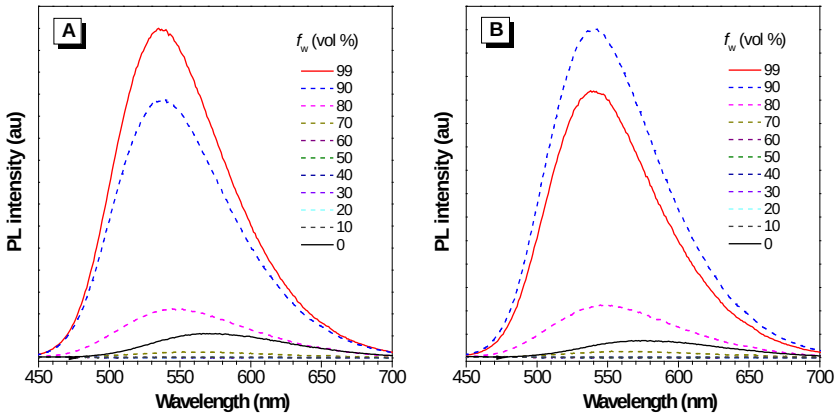

Figure S4. PL spectra of (A) 9-CCP-BP-PXZ and (B) 3,9-CCP-BP-PXZ in THF/water mixtures with different water fractions (f_w).

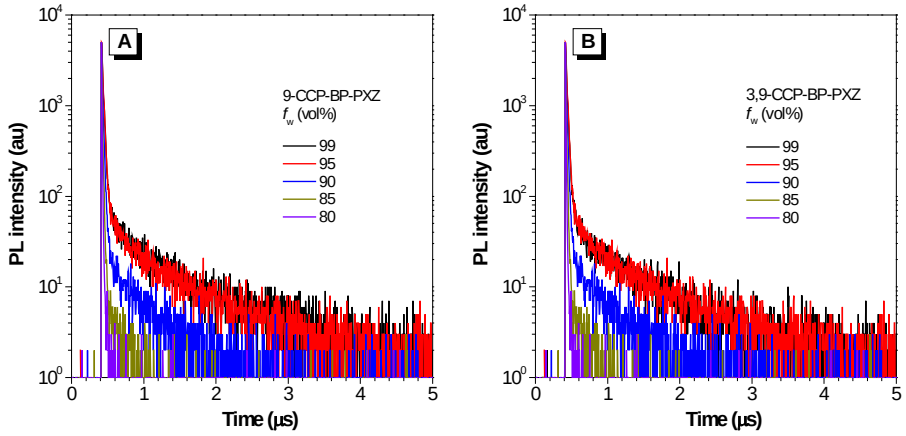

Figure S5. Transient PL decay spectra of (A) 9-CCP-BP-PXZ and (B) 3,9-CCP-BP-PXZ in THF/water mixtures with different water fractions (f_w).

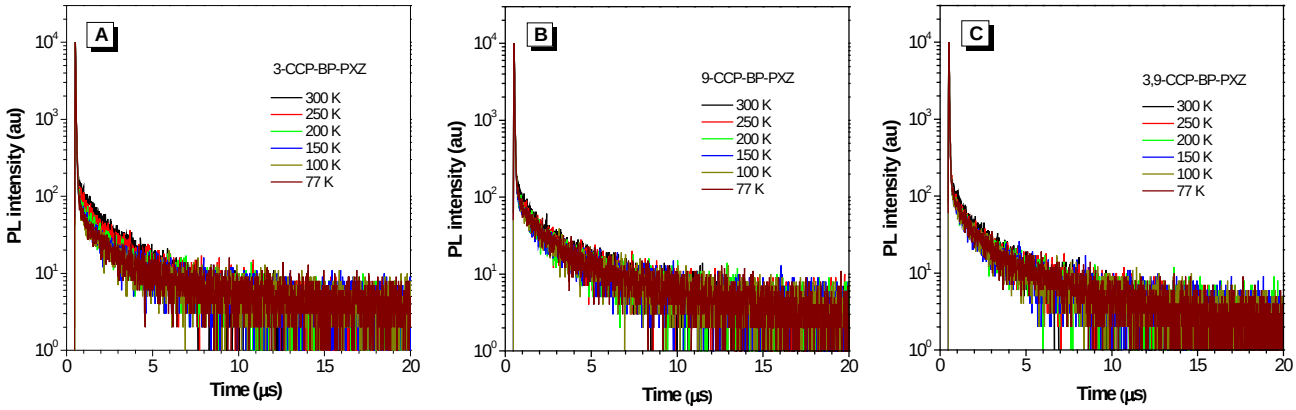

Figure S6. Temperature-dependent transient PL decay spectra of neat films of (A) 3-CCP-BP-PXZ, (B) 9-CCP-BP-PXZ and (C) 3,9-CCP-BP-PXZ under nitrogen.

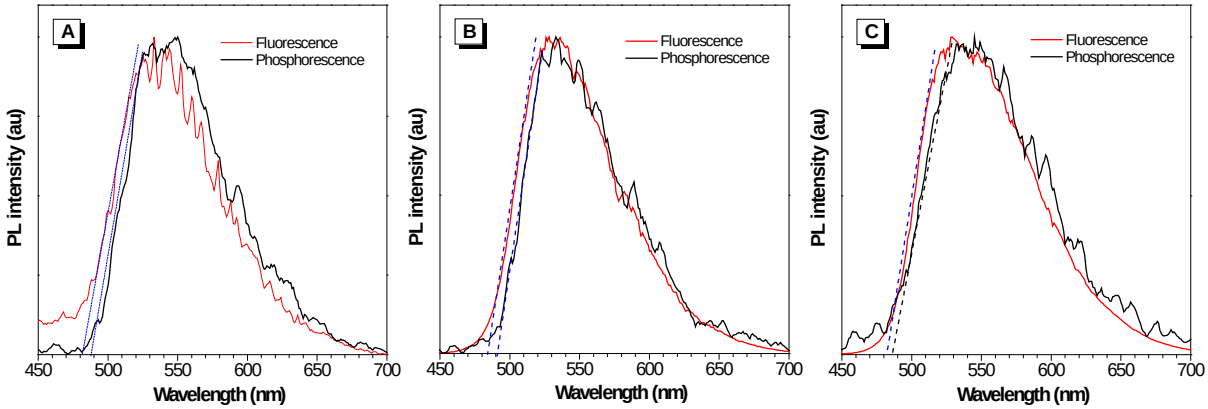

Figure S7. Fluorescence and phosphorescence spectra of the neat films of (A) 3-CCP-BP-PXZ, (B) 9-CCP-BP-PXZ and (C) 3,9-CCP-BP-PXZ, measured at 77 K under nitrogen.

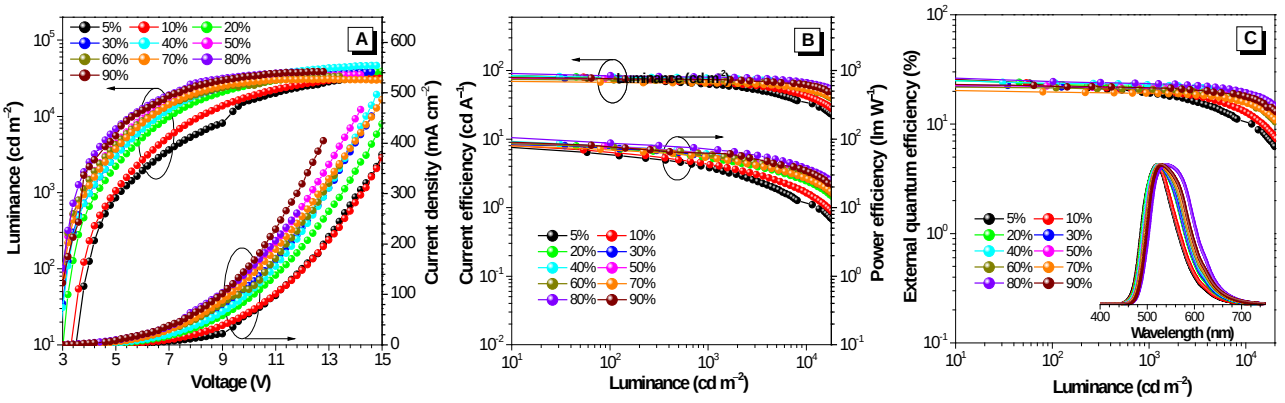

Figure S8. Plots of (A) luminance–voltage–current density, (B) current efficiency–luminance–power efficiency and (C) external quantum efficiency–luminance of the doped devices based on 9-CCP-BP-PXZ. Inset: EL spectra at 1000 cd m^{-2}. Device configuration: ITO/HATCN (5 nm)/TAPC (30 nm)/TCTA (5 nm)/9-CCP-BP-PXZ (*x* wt%) : CBP (20 nm)/TmPyPB (40 nm)/LiF (1 nm)/Al; *x* = 5, 10, 20, 30, 40, 50, 60, 70, 80 or 90.

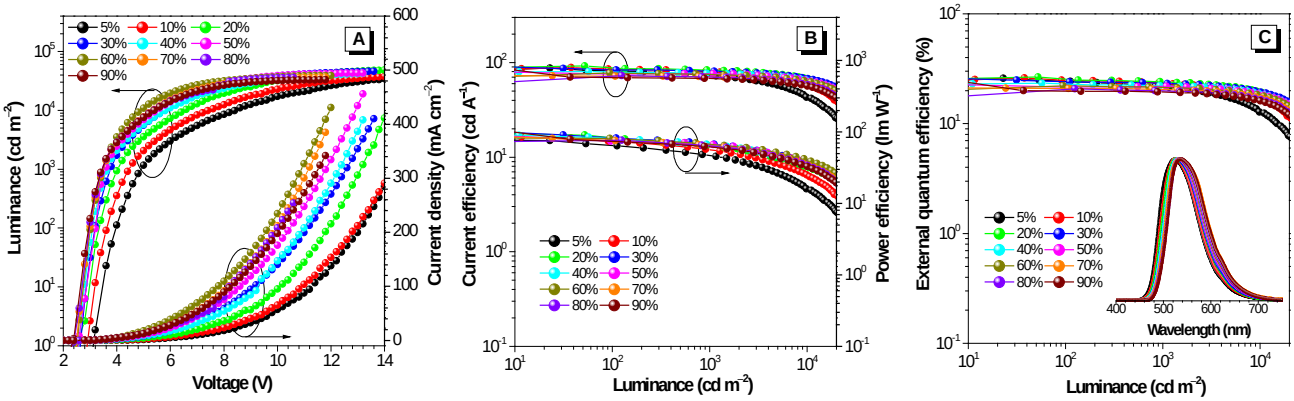

Figure S9. Plots of (A) luminance–voltage–current density, (B) current efficiency–luminance–power efficiency and (C) external quantum efficiency–luminance of the doped devices based on 3,9-CCP-BP-PXZ. Inset: EL spectra at 1000 cd m^{-2}. Device configuration: ITO/HATCN (5 nm)/TAPC (30 nm)/TCTA (5 nm)/3,9-CCP-BP-PXZ (*x* wt%) : CBP (20 nm)/TmPyPB (40 nm)/LiF (1 nm)/Al; *x* = 5, 10, 20, 30, 40, 50, 60, 70, 80 or 90.

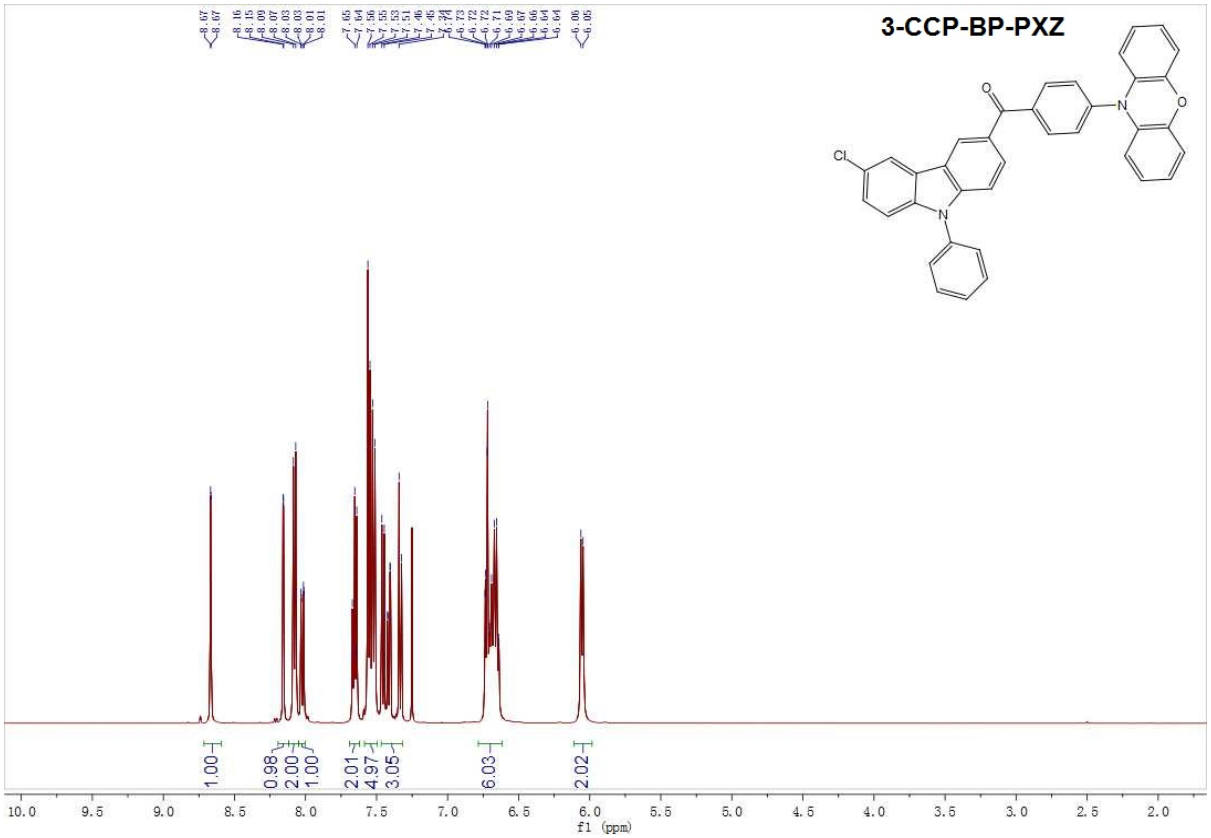

Figure S10. ^{1}H NMR spectrum of 3-CCP-BP-PXZ in $CDCl_3$.

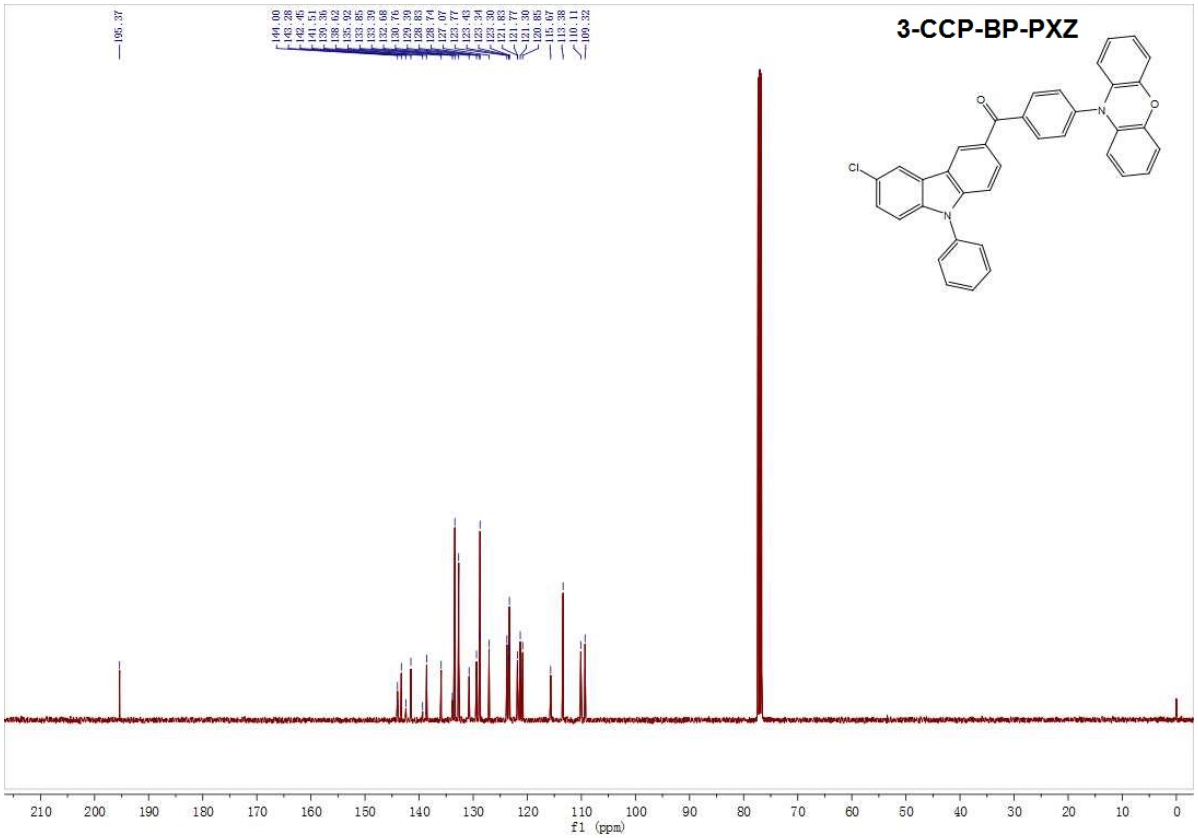

Figure S11. ^{13}C NMR spectrum of 3-CCP-BP-PXZ in $CDCl_3$.

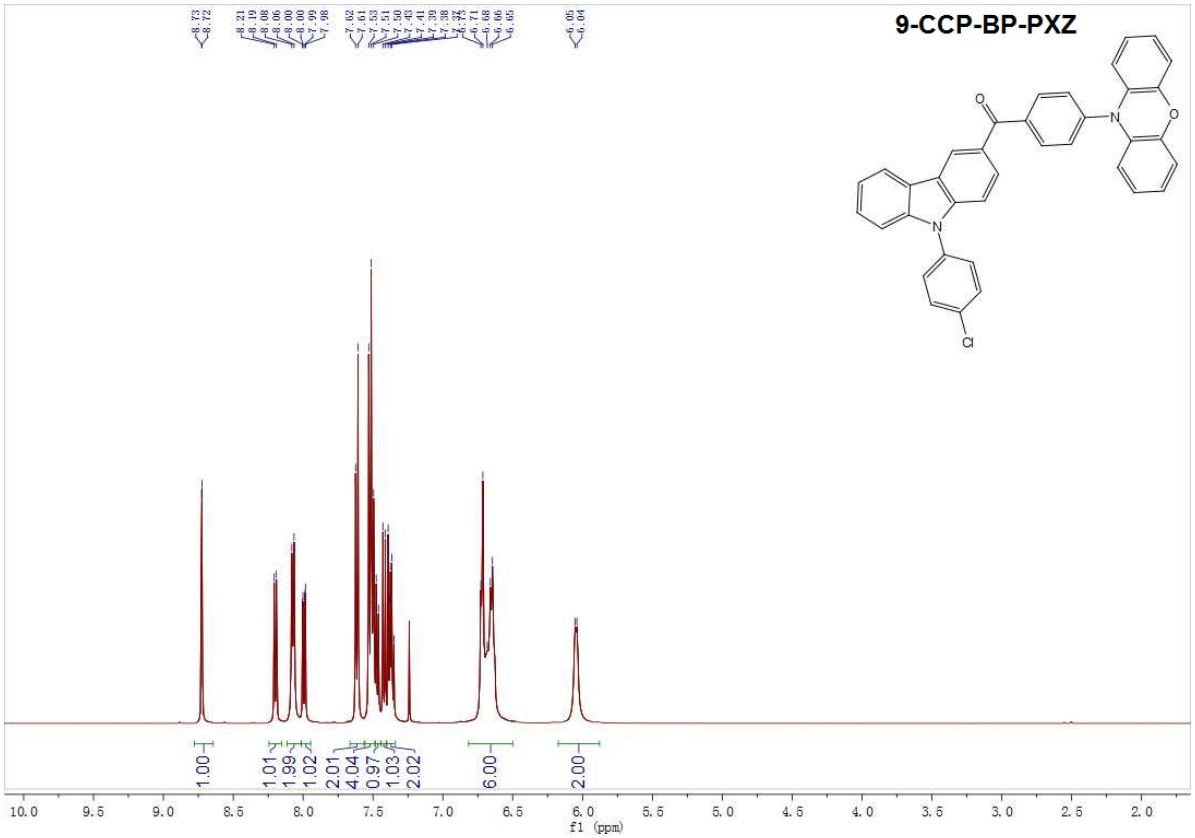

Figure S12. ^{1}H NMR spectrum of 9-CCP-BP-PXZ in $CDCl_3$.

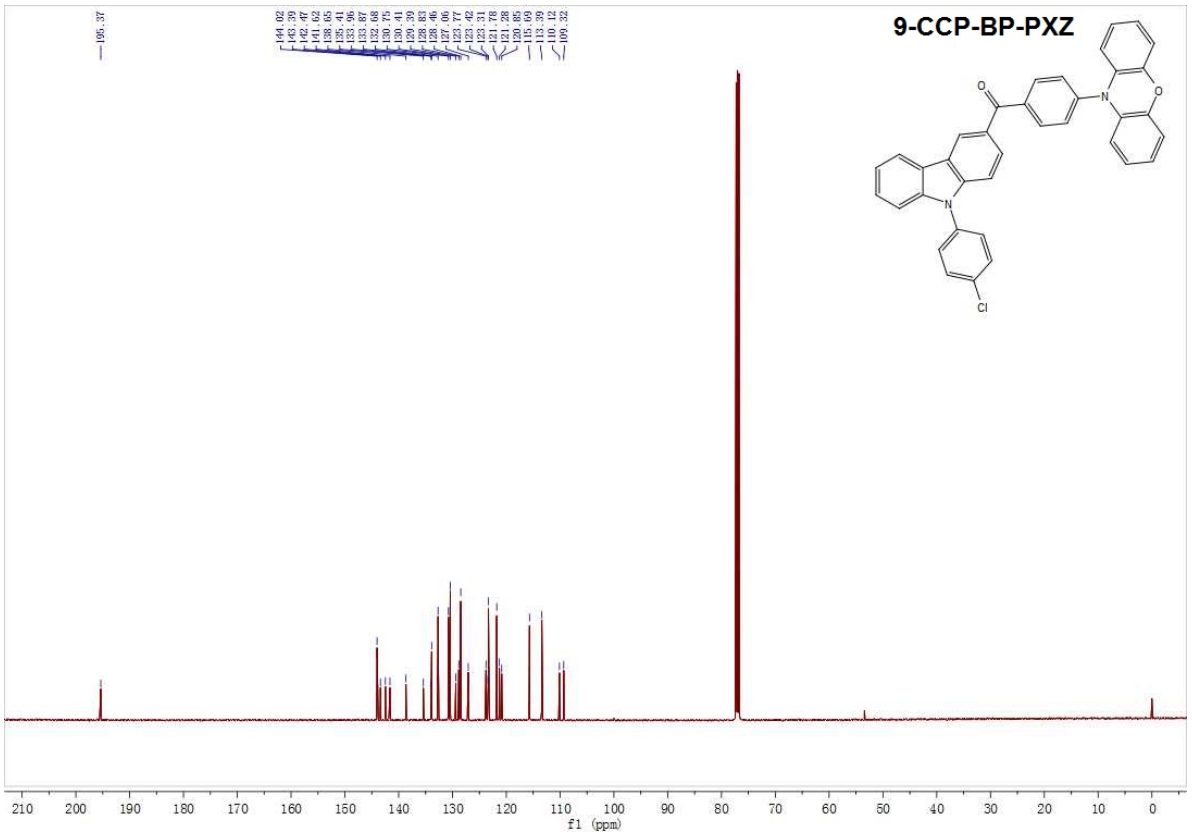

Figure S13. ^{13}C NMR spectrum of 9-CCP-BP-PXZ in $CDCl_3$.

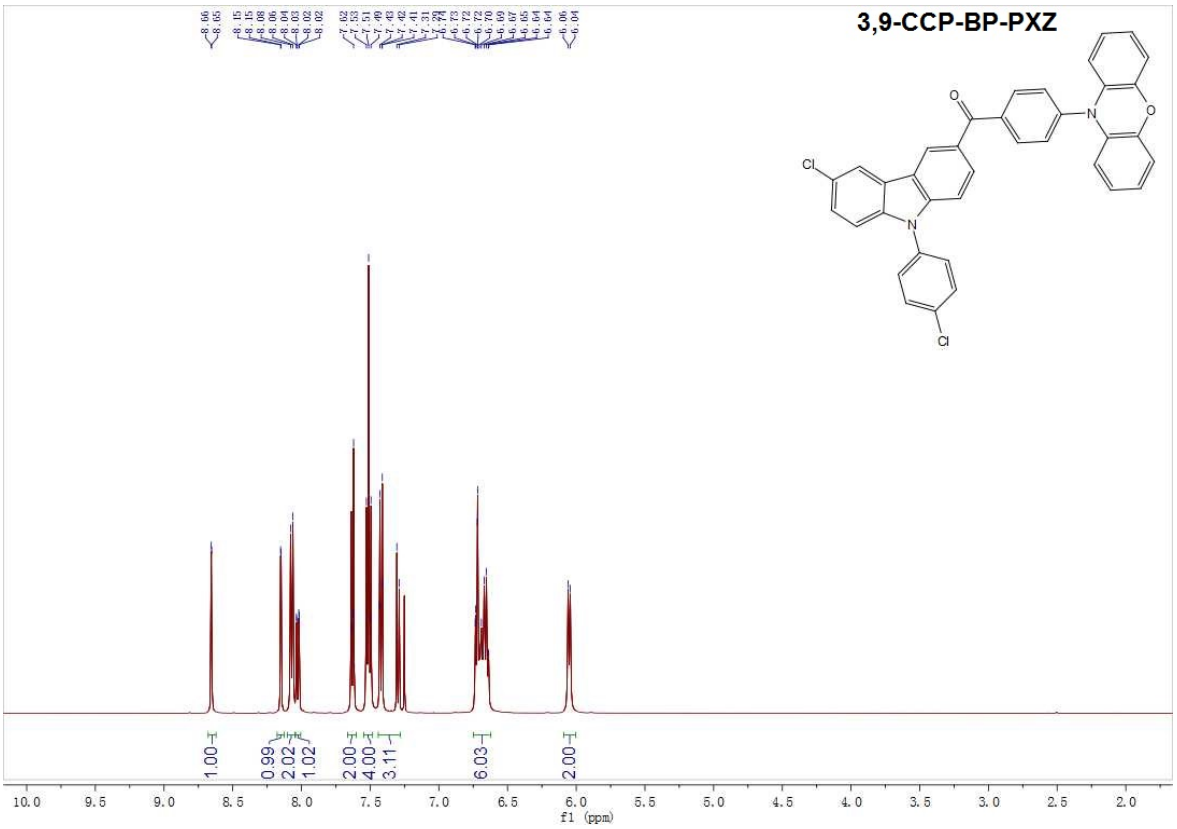

Figure S14. ^{1}H NMR spectrum of 3,9-CCP-BP-PXZ in $CDCl_3$.

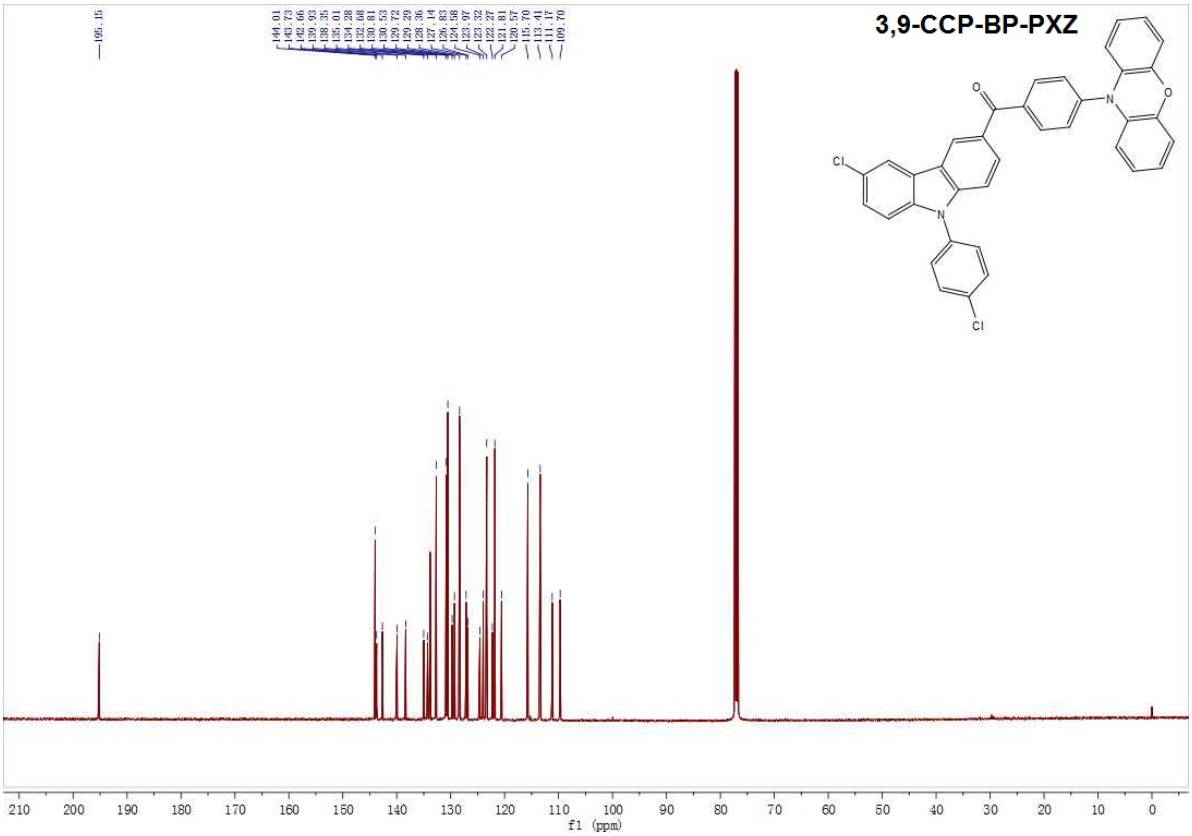

Figure S15. ^{13}C NMR spectrum of 3,9-CCP-BP-PXZ in $CDCl_3$.

Table S1. Transient PL decay data of 3-CCP-BP-PXZ, 9-CCP-BP-PXZ and 3,9-CCP-BP-PXZ in THF solution and in THF/water mixture with a water fraction (f_w) of 99 vol%.[a]

	f_w	$<\tau>$ (ns)	τ_1 (ns)	τ_2 (ns)	A_1	A_2	R_{prompt} (%)	$R_{delayed}$ (%)	λ_{em} (nm)
3-CCP-BP-PXZ	0	11.7	4.0	277.8	17361.9	7.2	97	3	575
	99	148.5	19.7	568.2	5311.0	56.4	76	24	539
9-CCP-BP-PXZ	0	10.3	2.8	163.5	9783.1	8.1	96	4	571
	99	153.9	20.7	653.4	6615.5	55.8	79	21	538
3,9-CCP-BP-PXZ	0	3.9	2.3	71.2	9928.6	7.7	98	2	576
	99	138.9	20.4	623.6	6410.5	51.3	80	20	540

[a]Transient PL decay data are fitted by double exponential function and the mean fluorescence lifetimes ($<\tau>$) were calculated by $<\tau> = \Sigma A_i\tau_i^2/\Sigma A_i\tau_i$, where A_i is the preexponential for lifetime τ_i. R_{prompt} and $R_{delayed}$ are individual component ratio for prompt and delayed fluorescence. $R_{prompt} = \tau_1A_1/(\tau_1A_1 + \tau_2A_2)$,[4] $R_{delayed} = 1 - R_{prompt}$.

Table S2. Photophysical data of the neat films of 3-CCP-BP-PXZ, 9-CCP-BP-PXZ and 3,9-CCP-BP-PXZ.[a]

	3-CCP-BP-PXZ	9-CCP-BP-PXZ	3,9-CCP-BP-PXZ
Φ_{PL} (%)	73.0	70.4	72.6
Φ_{prompt} (%)	55.5	52.6	56.1
$\Phi_{delayed}$ (%)	17.5	17.8	16.5
Φ_{ISC} (%)	24.0	25.2	22.8
τ_{prompt} (ns)	22.2	22.2	21.1
$\tau_{delayed}$ (μs)	0.76	0.68	0.42
$R_{delayed}$ (%)	24.0	25.2	22.7
k_F ($\times 10^6$ s^{-1})	25.0	23.7	26.6
k_{IC} ($\times 10^6$ s^{-1})	9.2	9.9	10.0
k_{ISC} ($\times 10^6$ s^{-1})	10.8	11.4	10.8
k_{RISC} ($\times 10^6$ s^{-1})	1.73	1.97	3.10

[a]Abbreviations: Φ_{PL} = absolute photoluminescence quantum yield; Φ_{prompt} and $\Phi_{delayed}$ = fluorescent and delayed components, respectively, determined from the total Φ_{PL} and the proportion of the integrated area of each component in the transient spectra to the total integrated area; Φ_{ISC} = the intersystem crossing quantum yield; τ_{prompt} and $\tau_{delayed}$ = lifetimes calculated from the prompt and delayed fluorescence decay, respectively; $R_{delayed}$ = the ratio of delayed component; k_F = fluorescence decay rate; k_{IC} = internal conversion decay rate from S_1 to S_0; k_{ISC} = intersystem crossing decay rate from S_1 to T_1; k_{RISC} = the rate constant of reverse intersystem crossing process.

Table S3. EL performance of the doped OLEDs based on 9-CCP-BP-PXZ.[a]

	V_{on}	maximum values				values at 1000 cd m^{-2}					
	(V)	η_C (cd A^{-1})	η_P (lm W^{-1})	η_{ext} (%)	L (cd m^{-2})	η_C (cd A^{-1})	η_P (lm W^{-1})	η_{ext} (%)	RO (%)	CIE (x,y)	λ_{EL} (nm)
5 wt%	3.4	77.6	64.1	23.6	36970	63.1	38.1	19.2	18.6	(0.28,0.59)	520
10 wt%	3.2	79.4	69.3	23.9	36520	67.4	42.4	20.3	15.1	(0.29,0.59)	521
20 wt%	2.8	76.6	79.1	22.9	39150	72.9	52.0	21.7	5.2	(0.32,0.58)	524
30 wt%	2.8	76.2	83.5	22.5	37990	71.3	56.0	21.1	6.2	(0.33,0.59)	527
40 wt%	2.8	81.3	85.1	24.1	46300	77.3	60.7	22.9	4.9	(0.34,0.58)	526
50 wt%	2.6	75.6	79.1	22.3	35000	71.8	59.3	21.2	4.9	(0.34,0.58)	526
60 wt%	2.6	75.2	90.8	22.0	33400	70.2	58.0	20.6	6.3	(0.35,0.59)	529
70 wt%	2.6	70.8	73.8	20.4	31690	68.4	56.5	19.9	2.4	(0.34,0.59)	529
80 wt%	2.6	77.3	80.9	22.5	38520	73.1	60.4	21.3	5.3	(0.36,0.58)	531
90 wt%	2.6	77.7	93.8	22.2	37370	72.1	62.8	20.6	7.2	(0.36,0.59)	532

[a]Abbreviations: V_{on} = turn-on voltage at 1 cd m^{-2}; η_C = current efficiency; η_P = power efficiency; η_{ext} = external quantum efficiency; L = luminance; RO = current efficiency roll-off from maximum value to that at 1000 cd m^{-2}; CIE = Commission Internationale de I'Eclairage coordinates. Device configuration: ITO/HATCN (5 nm)/TAPC (30 nm)/TCTA (5 nm)/emitter (20 nm)/TmPyPB (40 nm)/LiF (1 nm)/Al. emitter = 9-CCP-BP-PXZ (*x* wt%) : CBP; *x* = 5, 10, 20, 30, 40, 50, 60, 70, 80 or 90.

Table S4. EL performance of the doped OLEDs based on 3,9-CCP-BP-PXZ.[a]

Wt	V_{on}	maximum values				values at 1000 cd m^{-2}					
(%)	(V)	η_C (cd A^{-1})	η_P (lm W^{-1})	η_{ext} (%)	L (cd m^{-2})	η_C (cd A^{-1})	η_P (lm W^{-1})	η_{ext} (%)	RO (%)	CIE (x,y)	λ_{EL} (nm)
5 wt%	3.2	87.1	76.0	25.9	39100	72.2	45.4	21.5	16.9	(0.31,0.59)	522
10 wt%	3.0	88.9	84.6	26.0	39730	80.4	57.3	23.5	9.6	(0.32,0.59)	527
20 wt%	2.8	92.1	90.4	26.5	48760	83.4	65.1	24.0	9.4	(0.34,0.59)	528
30 wt%	2.8	90.3	101.3	25.9	46160	80.9	66.8	23.2	10.4	(0.35,0.59)	530
40 wt%	2.6	80.5	84.2	23.2	42310	76.8	67.0	22.2	4.3	(0.36,0.59)	532
50 wt%	2.6	79.6	89.3	22.8	43090	76.2	66.5	21.8	4.3	(0.36,0.59)	534
60 wt%	2.6	77.3	80.9	22.1	38940	74.1	64.7	21.2	4.1	(0.36,0.59)	534
70 wt%	2.6	73.6	88.9	21.4	36620	71.2	65.8	20.7	3.3	(0.38,0.58)	535
80 wt%	2.4	72.8	76.2	20.7	36270	70.4	65.0	20.0	3.4	(0.37,0.59)	536
90 wt%	2.4	70.1	78.6	20.0	33080	68.0	62.8	19.4	3.0	(0.38,0.58)	537

[a]Abbreviations: V_{on} = turn-on voltage at 1 cd m^{-2}; η_C = current efficiency; η_P = power efficiency; η_{ext} = external quantum efficiency; L = luminance; RO = current efficiency roll-off from maximum value to that at 1000 cd m^{-2}; CIE = Commission Internationale de I'Eclairage coordinates. Device configuration: ITO/HATCN (5 nm)/TAPC (30 nm)/TCTA (5 nm)/emitter (20 nm)/TmPyPB (40 nm)/LiF (1 nm)/Al. emitter = 3,9-CCP-BP-PXZ (*x* wt%) : CBP; *x* = 5, 10, 20, 30, 40, 50, 60, 70, 80 or 90.

Estimation of Basic Photophysical Data

The quantum efficiencies and rate constants were determined using the following equations according to Adachi's method (equations 1–7, 8 and 9–10).[5-7]

$$\Phi_{prompt} = \Phi_{PL}R_{prompt} \quad (1)$$

$$\Phi_{delayed} = \Phi_{PL}R_{delayed} \quad (2)$$

$$k_F = \Phi_{prompt}/\tau_{prompt} \quad (3)$$

$$\Phi_{PL} = k_F/(k_F + k_{IC}) \quad (4)$$

$$\Phi_{prompt} = k_F/(k_F + k_{IC} + k_{ISC}) \quad (5)$$

$$\Phi_{IC} = k_{IC}/(k_F + k_{IC} + k_{ISC}) \quad (6)$$

$$\Phi_{ISC} = k_{ISC}/(k_F + k_{IC} + k_{ISC}) = 1 - \Phi_{prompt} - \Phi_{IC} \quad (7)$$

$$\Phi_{RISC} = \Phi_{delayed}/\Phi_{ISC} \quad (8)$$

$$k_{RISC} = (k_p k_d \Phi_{delayed})/(k_{ISC}\Phi_{prompt}) \quad (9)$$

$$k_p = 1/\tau_{prompt}; \; k_d = 1/\tau_{delayed} \quad (10)$$

Reference

(1) Fan, J.; Lin, L.; Wang, C.-K. Excited State Properties of Non-doped Thermally Activated Delayed Fluorescence Emitters with Aggregation-Induced Emission: A QM/MM study. *J. Mater. Chem. C* **2017**, *5*, 8390-8399.

(2) Wu, Q. Y.; Deng, C. M.; Peng, Q.; Niu, Y. L.; Shuai, Z. G. Quantum Chemical Insights into the Aggregation Induced Emission Phenomena: A QM/MM Study for Pyrazine Derivatives. *J. Comput. Chem.* **2012**, *33*, 1862-1869.

(3) Forrest, S. R.; Bradley, D. D.; Thompson, M. E. Measuring the Efficiency of Organic Light-Emitting Devices. *Adv. Mater.* **2003**, *15*, 1043-1048.

(4) Nakagawa, T.; Ku, S.-Y.; Wong, K.-T.; Adachi, C. Electroluminescence Based on Thermally Activated Delayed Fluorescence Generated by a Spirobifluorene Donor-Acceptor Structure. *Chem. Commun.* **2012**, *48*, 9580.

(5) Zhang, Q.; Kuwabara, H.; Potscavage, W. J.; Huang, S.; Hatae, Y.; Shibata, T.; Adachi, C. Anthraquinone-Based Intramolecular Charge-Transfer Compounds: Computational Molecular Design, Thermally Activated Delayed Fluorescence, and Highly Efficient Red Electroluminescence. *J. Am. Chem. Soc.* **2014**, *136*, 18070-18081.

(6) Xie, G.; Li, X.; Chen, D.; Wang, Z.; Cai, X.; Chen, D.; Li, Y.; Liu, K.; Cao, Y.; Su, S.-J. Evaporation- and Solution-Process-Feasible Highly Efficient Thianthrene-9,9',10,10′-Tetraoxide-Based Thermally Activated Delayed Fluorescence Emitters with Reduced Efficiency Roll-Off. *Adv. Mater.* **2016**, *28*, 181-187.

(7) Uoyama, H.; Goushi, K.; Shizu, K.; Nomura, H.; Adachi, C. Highly Efficient Organic Light-Emitting Diodes from Delayed Fluorescence. *Nature* **2012**, *492*, 234-238.